3D-QSAR Studies on Cannabinoid CB1 Receptor Agonists: G-Protein Activation as Biological Data

Outi M. H. Salo,*,† Juha R. Savinainen,‡ Teija Parkkari,† Tapio Nevalainen,† Maija Lahtela-Kakkonen,† Jukka Gynther,† Jarmo T. Laitinen,‡ Tomi Järvinen,† and Antti Poso†

Departments of Pharmaceutical Chemistry and Physiology, University of Kuopio, P.O. Box 1627, FIN-70211 Kuopio, Finland

Received June 2, 2005

G-protein activation via the CB1 receptor was determined for a group of various CB1 ligands and utilized as biological activity data in subsequent CoMFA and CoMSIA studies. Both manual techniques and automated docking at CB1 receptor models were used to obtain a common alignment of endocannabinoid and classical cannabinoid derivatives. In the final alignment models, the endocannabinoid headgroup occupies a unique region distinct from the classical cannabinoid structures, supporting the hypothesis that these structurally diverse molecules overlap only partially within the receptor binding site. Both CoMFA and CoMSIA produce statistically significant models based on the manual alignment and a docking alignment at one receptor conformer. Leave-half-out cross-validation and progressive scrambling were successfully used in assessing the predictivity of the QSAR models.

Introduction

Cannabis sativa has been used for millenia for both recreational and medicinal purposes,[1] but its major psychoactive component (−)-*trans*-Δ^9-tetrahydrocannabinol (Δ^9-THC, **1**, Table 1) was isolated and identified only in the 1960s.[2] In the following years, numerous analogues of the classical plant cannabinoids were synthesized and tested for their biological activity to elucidate the structure−activity relationships (SAR) of cannabinoids.[3] Also, new structural groups of cannabimimetic ligands were discovered and developed; nonclassical cannabinoids[4] typified by (1*R*,3*R*,4*R*)-3-[2-hydroxy-4-(1,1-dimethylheptyl)phenyl]-4-(3-hydroxypropyl)cycl ohexan-1-ol (**3**, CP55940, Table 1), and aminoalkylindoles[5] (AAIs) typified by (*R*)-(+)-[2,3-dihydro-5-methyl-3-[(4-morpholinyl)methyl]pyrrolo[1,2,3-*de*]-1,4-be nzoxazin-6-yl]-(1-naphthalenyl)methanone (WIN55212-2, Figure 1). However, the recent discovery of the endogenous cannabinoid system (ECS) comprising the cannabinoid receptors,[6,7] endogenous ligands,[8−13] and enzymes for ligand metabolism[14,15] has triggered intensive research into the therapeutic potential of cannabinergic ligands. For example, the receptor agonists targeted at CB1, the central receptor subtype, have a wide range of potential applications including nausea, glaucoma, cancer, stroke, pain, cachexia, and neuronal disorders such as multiple sclerosis and Parkinson's disease.[16] Conversely, CB1 antagonists typified by the diarylpyrazole rimonabant[17] (SR141716A, Figure 1) have shown potential in the management of obesity and nicotine dependence.[16]

There are several approaches used in the development of therapeutically useful cannabinergic ligands (i.e., ligands that act on the enzymes or receptors of the ECS). For example, various computational methods have been used to probe the structure of the ligand binding site of the target proteins, especially the cannabinoid receptors (recently reviewed in ref 18). Comparative molecular field analysis[19] (CoMFA), a three-dimensional quantitative structure−activity relationship (3D-QSAR) method that utilizes ligand SAR, has been employed to obtain indirect information about the CB1 binding site. The reported CoMFA models are based either on SAR from one structural class of ligands[20−26] or from two or more classes of ligands.[27−30] For the latter models, research groups have attempted to derive common pharmacophoric alignments of structurally different cannabinergic ligands, based on the fact that the ligands displace one another in radioligand binding assays.[22,28,30−37] Commonly, CB1 receptor binding affinities or, in some cases, in vivo pharmacological potencies have been used as biological activity data in the 3D-QSAR models. Although the binding affinities of many ligands may in general correlate well with in vivo activities,[38] there is a recognized disparity between the two properties of affinity and efficacy.[39,40] The classical radioligand binding assay cannot reveal if a molecule is an agonist or an antagonist.[41] This knowledge is valuable especially when incorporating novel, pharmacologically uncharacterized structures into a QSAR model. With respect to G-protein coupled receptors (GPCRs) such as CB1, the GTPγS binding assay has been demonstrated to be effective at measuring efficacy differences between ligands.[42] To the authors' knowledge, there are not many published studies that utilize G-protein activation as biological data in 3D-QSAR models. Recently, Francisco et al.[21] generated CoMFA models for amide and hydrazide analogues of SR141716A using both cannabinoid receptor affinity and efficacy measured in the GTPγS binding assay as biological activity data. However, a statistically significant model could be produced only with the CB1 binding affinitiess although, in general, the level of G-protein activation (EC_{50} values) paralleled the observed trends in CB1 receptor affinity. Rivara et al.[43] successfully used the intrinsic activity measured in the GTPγS binding assay to build CoMFA models for a set of melatonin receptor ligands.

The aim of the present study was to create a statistically significant 3D-QSAR model that could further be utilized in the design of novel selective CB1 agonists. Both classical and endogenous cannabinoid ligand derivatives were chosen for the model, as they are thought to bind to the same or at least partially to the same site in the CB1 receptor binding cavity.[44,45] Among the endocannabinoid derivatives, we included some recently synthesized molecules, such as reversed amide derivatives[46] of

* To whom correspondence should be addressed. Tel: +358-17-163714. Fax: +358-17-162456. E-mail: outi.salo@uku.fi.
† Department of Pharmaceutical Chemistry.
‡ Department of Physiology.

10.1021/jm0505157 CCC: $33.50
Published on Web 12/21/2005

Table 1. Molecular Structures and G-Protein Activation Data Used in the 3D-QSAR Models

No	Structure	Potency[a]	No	Structure	Potency
1	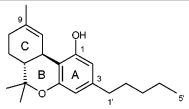	6.7	**2**	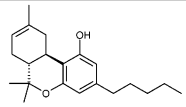	6.2
3	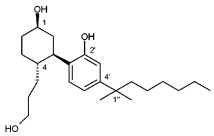	7.0	**4**	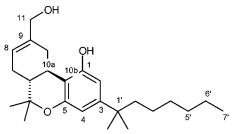	8.3
5	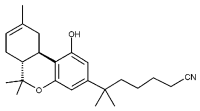	8.0	**6**	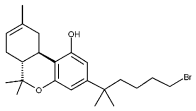	8.0
7	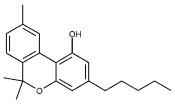	6.5	**8**	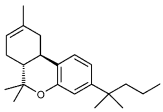	5.7
9	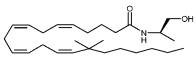	5.9[b]	**10**	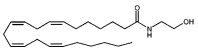	4.7[b]
11	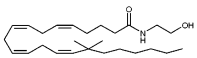	6.0[b]	**12**	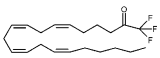	4.6
13	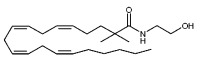	5.1[b]	**14**	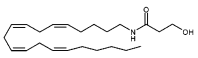	5.1
15	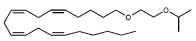	5.9[c]	**16**	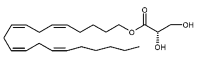	4.4
17	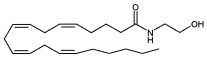	4.8	**18**	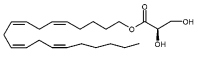	4.6
19	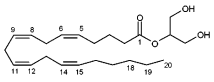	5.5[b]	**20**	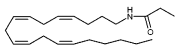	5.7
21	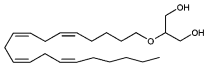	4.9[c]	**22**	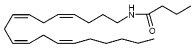	5.9
23	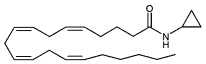	6.4	**24**	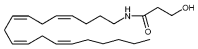	4.8
25	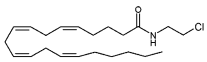	6.5	**26**	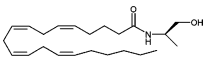	5.1[c]
27	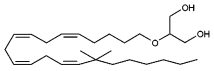	4.4	**28**	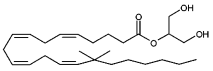	4.3
29	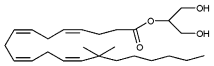	4.3	**30**	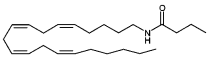	5.5
31	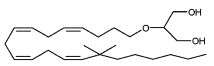	4.3[d]	**32**	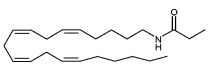	5.5

[a] pEC_{50}: mean of at least three independent experiments performed in duplicate; see Supporting Information (section A) for detailed presentation of the G-protein activation data. [b] Reported previously in ref 47. [c] Reported previously in ref 90; pEC_{50} at GDP concentration of 10^{-5} M. [d] Mean of two independent experiments performed in duplicate.

N-arachidonoylethanolamide[8] (AEA, **17**, Table 1) and dimethylheptyl (DMH) side-chain analogues[47] of 2-arachidonoylglycerol[9,10] (2-AG, **19**, Table 1). In addition to the manual alignment model based on the pharmacophoric elements of the ligands, several docking alignments were created with the help of different CB1 model conformations reported previously by us.[48] CoMFA[19] and CoMSIA[49−51] (comparative molecular similarity index analysis) interaction fields were calculated for each set

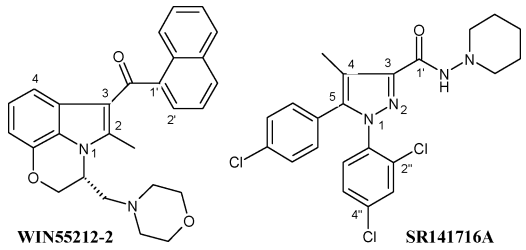

Figure 1. Molecular structures of a prototype aminoalkylindole WIN55212-2 and a diarylpyrazole CB1 antagonist SR141716A.

of differently aligned molecules, and the resulting 3D-QSAR models were validated using both different-sized cross-validation groups and progressive scrambling.[52,53]

Results and Discussion

G-Protein Activation Data. The CB1 receptor mediated G-protein activation data of 32 CB1 receptor ligands (**1**−**32**) is presented in Table 1 (see Supporting Information, section A, for more detailed results). Initially, since the resulting biological data from the [^{35}S]GTPγS binding assay provides (i) efficacy (maximal agonist response, E_{max}, %basal) and (ii) potency (pEC_{50}), we wanted to use both of these values as dependent variables in separate 3D-QSAR models. We were attracted to this approach by the fact that a potency value does not reveal any data about the maximal response of the ligand. For example, in the present study the potency of **4** (HU-210) was 8.3 and its E_{max} 396% of the basal level (100%) of G-protein activation in rat cerebellar membranes, while the corresponding values for **1** were 6.7/159%, and for **19** 5.5/561%. One can see that, in the present system, **4** is a very potent ligand but the significantly less potent compound, **19**, produces the highest maximal response, whereas **1** is the least efficacious of these three compounds. However, with this data it was not possible to derive statistically significant CoMFA/CoMSIA models with predictive power for the E_{max} values (see Supporting Information, sections A, J, and K), and thus we used the pEC_{50} values in the final models. Moreover, molecule **31** was omitted from the final analyses as, in its case, the number of independent activity experiments (n) was only two (for the other compounds $n = 3$ or more). This did not significantly affect the statistical values of the QSAR models (Supporting Information, section H).

Manual Alignment of Ligands. To superimpose the classical and endogenous cannabinoid derivatives, a template molecule was selected from both structural classes: **4**, a potent synthetic analogue of classical cannabinoids served as a rigid template structure for the whole alignment process, whereas **19**, being a full CB1 agonist,[54] was used as a template for the endocannabinoid structures. The alignment process was guided by the fact that the aliphatic side chain of classical cannabinoids is one of the most crucial pharmacophoric groups and it seems to correspond to the C16−C20 saturated region of the endocannabinoids.[55,56] Other criteria for superimposing the structural templates were (i) good steric overlap, (ii) reasonably close matching of other pharmacophoric elements (hydrogen bond acceptor/donor areas and π-electron rich areas), and (iii) the ability of an alignment to sensibly incorporate **3** and two semirigid molecules which activate G protein via the CB1 receptor[57] (see Supporting Information, sections C−F).

In the final alignment (Figure 2), the **4** side chain is oriented almost perpendicularly to the plane of the aromatic A ring. This orientation is supported, for example, by the study of Busch-Petersen et al.[58] They synthesized a series of unsaturated side chain analogues of β-11-OH-hexahydrocannabinol (HHC) and

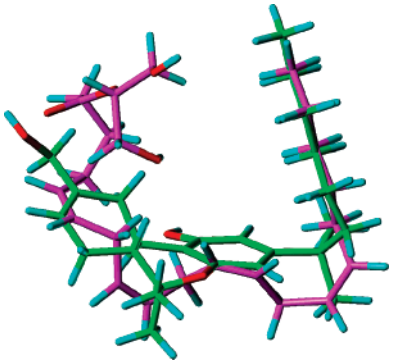

Figure 2. Manual alignment of the U-shaped **19** (magenta) and **4** (green). Hydrogen atoms are colored with cyan and oxygen atoms with red. The polar headgroup of **19** is pointing toward the viewer.

reported that an analogue with a *cis*-hept-1-ene side chain had the highest affinity for CB1. The results from their conformational analysis showed that this side chain would adopt the same kind of orientation as a DMH side chain (cf. ref 59) running perpendicularly to the plane of the aromatic ring and being in closest proximity with this ring when compared with the other analogues. Similarly, Khanolkar et al.[60] demonstrated that forcing the cannabinoid side chain into a lateral orientation and further away from the aromatic ring decreased significantly the CB1 affinities. Busch-Petersen and coauthors[58] also pointed out that the *cis*-hept-1-ene side chain is notably similar to the last seven carbons of the arachidonic acid portion of **17**.

In the first CoMFA study reported for **17** and its derivatives, Thomas et al.[28] identified a J-shaped or looped conformation to be energetically favorable and well superimposable with the classical cannabinoids. Subsequently, Tong et al.[35] proposed a helical conformer of **17** to be the pharmacophoric conformation of this endocannabinoid. On the basis of these proposed conformations, Howlett and co-workers[25] developed two separate CoMFA models for a set of endocannabinoid derivatives. When comparing solely the resulting CoMFA models, however, it was not possible to determine which of these conformations would be favored. In the present study, a U-shaped conformation of **19** was chosen as the template for the endocannabinoid derivatives (Figure 2). This choice is supported by the observation that analogues of **17** which are capable of forming tightly curved (U-shaped) structures are associated with higher CB1 affinity.[61,62] Also, conformational memories (CM) studies by Barnett-Norris et al.[61] showed that both extended shape and U-shape are major conformational families of **17** and **19** in both $CHCl_3$ and water. For a DMH derivative of **17**, the U-shape was predominant in both environments.

Both Thomas et al.[28] and Tong et al.[35] aligned the alkyl side chain and the polyolefin loop of **17** with the C3 pentyl chain and the tricyclic ring system of classical cannabinoids. The former authors, however, superimposed the carboxyamide oxygen of **17** with the pyranyl oxygen of **1** and the headgroup hydroxyl of **17** with the C1 phenolic hydroxyl of **1**, whereas the latter authors overlaid the corresponding elements of **17** with the C1 phenolic hydroxyl and C9 hydroxyl of 9-nor-9β-OH-HHC, respectively. Khanolkar et al.[63] demonstrated that the amide oxygen is important for the CB1 binding affinity of **17** and its analogues, but the synthesis of potent nonclassical cannabinoids which lack the pyran ring proved that the pyranyl oxygen was not essential for cannabinoid activity.[4,64] On the other hand, there is experimental evidence that neither the C1 phenolic hydroxyl[65] nor the headgroup hydroxyl of **17**[66,67] is essential for cannabinoid activity, although molecules do need to have an oxygen atom capable of forming a hydrogen bond

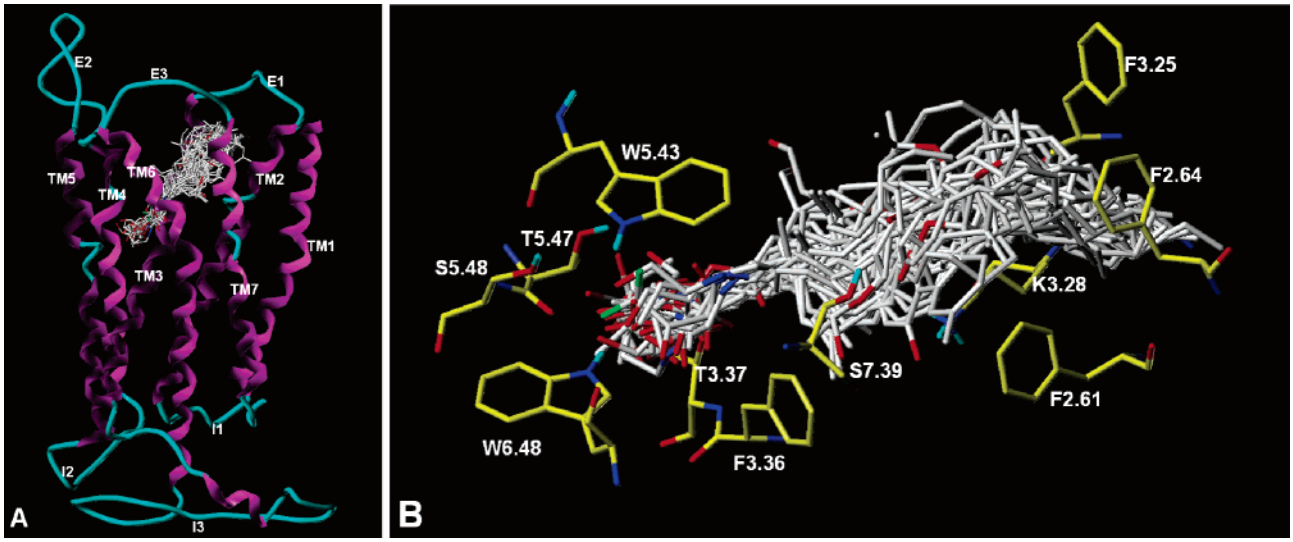

Figure 3. Docking alignment at model 3. (A) Endocannabinoid headgroup dives deep down into the binding cavity, whereas the endocannabinoid acyl chain and the classical cannabinoid derivatives occupy the upper region within the transmembrane bundle. TM1−7, transmembrane helices; E1−3, extracellular loops; I1−3, intracellular loops. (B) Residues surrounding the docked CB1 ligands.

to K3.28(192). The recent results of Martin et al. 2002[68] imply that the phenolic hydroxyl and the headgroup hydroxyl of **17** do not overlap. Also, Huffman et al.[69] synthesized pyridone analogues of classical cannabinoids which provide evidence that the amide oxygen of **17** does not substitute for the phenolic hydroxyl of classical cannabinoids in interactions with the CB1 receptor.

Due to the above-described difficulties in identifying the common pharmacophoric alignment of the polar groups, we did not deliberately try to find one single alignment. Even though we used reasonably close positioning of the polar areas as one criterion for the choice of the alignment, more emphasis was placed on the steric overlap and the matching of the alkyl side chains. Therefore, in the present alignment, the alkyl side chains of **4** and **19** match well and the polyolefin loop of **19** follows closely the tricyclic ring system of **4**. In particular, the C11−C12 and C5−C6 double bonds of **19** are overlaid with the π-electron rich areas of **4**. The lone pair electrons (LPs) of the C11 hydroxyl of **4** reach into the same region with the LPs of the ester group of **19**. When aligning all the other CB1 ligands according to their structural templates, the C1 hydroxyl of **3** was positioned near to the other polar atoms of the endocannabinoid headgroup region. Here, the phenolic hydroxyl of the cannabinoid derivatives and the southern aliphatic hydroxyl (SAH, C4 hydroxypropyl) of **3** do not have any counterpart among the functional groups of the endocannabinoid derivatives. It should be noted that the region of steric interference behind the C9 substituent of classical cannabinoids[70,71] was also kept free in the present superimposition.

Docking Alignments. Molecular docking to target protein structures has successfully been used as an automated alignment method in creating 3D-QSAR models. Docking at both protein crystal structures[72−75] and comparative (homology) models[76−78] has resulted in statistically significant and predictive QSAR models. In the absence of a precise pharmacophore, automated docking can be a useful tool for generating an alignment that is not biased by the preconceived ideas of a researcher. Here, we used seven different receptor conformers (models 1−7) of the previously reported rhodopsin crystal structure based CB1 comparative model[48] to derive automated alignments for the CB1 ligands. As described in our previous study, we had not sought to model the extracellular loops precisely, since it is not possible to determine their exact conformation without an experimental receptor structure. It is evident that especially the second extracellular loop (E2) of CB1 is different from the rhodopsin crystal structure[79] in which the E2 loop covers the ligand binding site. Specifically, besides the different length of the loop, CB1 lacks the conserved disulfide bridge between the third transmembrane helix (TM3) and the E2 loop. Hurst et al.[115] proposed that, due to these differences, the E2 loop of CB1 would occupy less volume in the upper part of the binding pocket than does the E2 loop in rhodopsin. In the present study, all receptor models 1−7 have an E2 loop that does not cover the putative ligand binding site. Molecular dynamics (MD) simulations performed with our CB1 model suggest that this open form of the loop is energetically stable (data not shown), although it would not represent the true conformation.

Model 1 was earlier described to accommodate a set of known CB1 agonists, whereas the CB1 antagonist SR141716A was docked well into model 7.[48] Interestingly, in the present study the docking alignment with model 3 produced the best QSAR models of all the alignments created by docking (see Supporting Information, section H). It seems likely that the fuzzy alignment of the endocannabinoid derivatives with model 1 was the source of the statistical instability in the CoMFA and CoMSIA based on that alignment. In all other receptor models except for models 6 and 7, the proposed "toggle switch" residues for CB1 activation[80] (F3.36/W6.48) had their χ1 torsional angles at gauche+/trans rotameric states (i.e., "active" state), respectively. In model 6, the corresponding rotameric states were trans/trans ("intermediate" state), and in model 7 trans/gauche+ ("inactive" state). At this point, it is important to mention that this simple change in the side chain conformations of the binding site residues is naturally not enough to bring a receptor to an active state, since it is evident from the experimental studies of other GPCRs that, for example, rearrangement of TM helices 3 and 6 is necessary for the receptor activation (for a review, see ref 81).

In the present docking alignment with model 3, the endocannabinoid derivatives are mostly in an extended or L-shaped conformation and their polar headgroup reaches deep down into the binding cavity (Figure 3A). Aromatic residues such as W6.48(356), W5.43(279), and F3.36(200) surround the headgroup region within a radius of 2.5 Å (Figure 3B). Both

Table 2. Statistics of CoMFA and CoMSIA PLS Analyses[a]

		CoMFA					CoMSIA				
model alignment	cv[b]	q^2 [c]	S_{PRESS}[d]	N[e]	r^2 [f]	S[g]	q^2	S_{PRESS}	N	r^2	S
MA[h]	LHO	0.455	0.851	3	0.881	0.401	0.521	0.773	1	0.699	0.615
	LSO	0.535	0.790	3	–[i]	–	0.601	0.731	3	0.916	0.338
		0.586	0.759	4	0.937	0.297	0.634	0.714	4	0.950	0.264
	LOO	0.688	0.674	5	0.958	0.247	0.700	0.662	5	0.972	0.200
model 3[j]	LHO	0.521	0.782	2	0.934	0.293	0.484	0.814	2	0.915	0.334
		0.555	0.767	3	0.981	0.159					
	LSO	0.695	0.641	3	–	–	0.628	0.695	2	–	–
	LOO	0.736	0.597	3	–	–	0.662	0.663	2	–	–

[a] pEC_{50} of G-protein activation via the CB1 receptor was used as biological activity data for the set of 31 cannabinoid ligands. [b] Cross-validation method; LHO = leave-half-out; LSO = leave-some-out (20%); LOO = leave-one-out. [c] Cross-validated correlation coefficient; for LHO and LSO mean of 20 independent analyses. [d] Standard error of prediction; for LHO and LSO mean of 20 independent analyses. [e] Number of PLS components. [f] Conventional (nonvalidated) correlation coefficient. [g] Standard error of estimate. [h] Manual alignment. [i] Determined above. [j] Docking alignment at the CB1 comparative model 3 (see ref 48).

tryptophan residues, as well as T3.37(201), T5.47(283), and S5.48(284), are capable of forming hydrogen bonds with the hydroxyl or carbonyl groups of the endocannabinoid derivatives. For example, the carbonyl group of **17** forms hydrogen bonds with W5.43(279) and W6.48(356), and the hydroxyl group with T3.37(201). Also, a headgroup intramolecular H-bond, as in the case of **27**, can help the hydroxyl groups to exist in such a hydrophobic region.[62] In addition, this hydrophobic receptor subsite that interacts with the endocannabinoid headgroup is fairly confined. This is in agreement with the experimental SAR for the endocannabinoid headgroup: both hydrophobic and electronegative headgroup substituents are allowed,[82] whereas introduction of large headgroups is not well tolerated by the CB1 receptor.[83] In the present alignment, for example, **13** did not fit into the subsite because of the presence of the dimethyl substituent at C2.

The present docking mode of the endocannabinoid ligands at the receptor model 3 differs from that which was previously reported by us at the receptor model 1[48] and from that reported by McAllister et al.[45] According to the model of McAllister and co-workers, **17** hydrogen bonds with K3.28(192) and has a C−H···π interaction with F3.25(189). Also, mutational studies have shown that replacing F3.36(200), W5.43(279), or W6.48-(356) with alanine did not affect the CB1 affinity of **17** or **3**,[80] although full receptor activation by these ligands could only be produced at W6.48A, but not F3.36A or W5.43A mutants. Thus, it has been suggested that these aromatic residues would not be part of the binding site of **17** or **3**. Consistent with the mutational data and the modeling studies of McAllister et al.,[45] **3** and the classical cannabinoid derivatives do not occupy the above-described subsite but position themselves, together with the endocannabinoid acyl chain, in the upper region of the transmembrane helix (TMH) bundle. The only exception is **8** (JWH-133), a selective CB2 agonist, since its C ring protrudes into the same site with the endocannabinoid headgroup (see Supporting Information, section G). On the whole, the classical cannabinoid derivatives adopted greater variety of configurations and orientations than the endocannabinoid derivatives. In his review on the side chain modifications of cannabinoid analogues, Seltzman[84] suggested that the tricyclic structure of classical cannabinoids would be positioned differently in the receptor for each different side chain. This could, indeed, be one reason for the variety of docking orientations of the cannabinoid analogues noted in the present study (Supporting Information, section G).

Lysine K3.28(192) that has been reported to be an essential residue for the binding of **17**, **4**, and **3**[44] does not form any hydrogen bonds with the ligands docked at model 3. However, K3.28(192) is engaged in cation−π interactions[85] with the aromatic A ring of all the cannabinoid analogues, except for **8**. In all cases, the aromatic ring centroid is within a 5 Å distance from the lysine NZ or CE atoms. Such interactions might also be possible between K3.28(192) and the nearby acyl chain double bond electrons of the endocannabinoid derivatives.

Additionally, we produced another docking alignment at a K3.28A mutant of model 3 to see if the residue was, indeed, important for the functional alignment of the ligands. This alignment could not produce a statistically valid QSAR model (Supporting Information, sections H and I), thus emphasizing the importance of this residue. We also tested if improving the relative alignment of the cannabinoid derivatives could affect the resulting QSAR models. According to CScore rank values, the next "best" conformers of **1**, **4**, **7**, and **8** that aligned well with the docking conformers of the other cannabinoid derivatives were chosen for the alignment. The same test was performed also on the K3.28A mutant receptor. However, the resulting QSAR models were statistically worse than the original alignment model (Supporting Information, sections H and I). In conclusion, even though the docking positions of the CB1 ligands may not be totally realistic, the alignment may still have realistic features which cause the resulting QSAR models to be statistically significant.

CoMFA and CoMSIA Statistics. CoMFA and CoMSIA models were derived for the manual alignment (MA) as well as for the different docking alignments. As already mentioned, only the docking alignment with model 3 (DA3) produced statistically significant QSAR models (see Supporting Information, section H for the detailed results of other docking models). Both MA and DA3 produced CoMFA/CoMSIA models with comparable PLS statistics (Table 2). MA CoMSIA resulted in slightly better q^2 and S_{PRESS} values than the MA CoMFA model, whereas the opposite was true for the DA3 models. The MA models seem to need more PLS components to explain the data compared with the DA3 models.

In the present study, the leave-one-out (LOO) cross-validation generally gave the highest q^2 values. Since LOO has often been described to give overly optimistic results, one should not blindly rely on it in assessing the predictive power of a QSAR model. Golbraikh and Tropsha[86] emphasized that high q^2 values, while being necessary, are not sufficient for endowing high predictive power to a model. They recommended the use of an external test set as the only way to establish a reliable QSAR model. For a typical QSAR setting with a small or modest sample size, however, Hawkins et al.[87] have argued that when validating such a model, it is better to use properly conducted cross-validation than to waste valuable information by holding back compounds for a test set. Therefore, we also performed leave-some-out (LSO; 5 random groups) and even a more stringent leave-half-

Table 3. Progressive Scrambling Statistics for CB1 QSAR Models Based Either on the Manual or Docking Alignment[a]

model	N[b]	$Q_s^{*2} \pm$ SD[c]	$Q_0^{*2} \pm$ SD[d]	$SDEP_s^* \pm$ SD[e]	$SDEP_0^* \pm$ SD[f]	$dq^2/dr_{yy}^2 \pm$ SD[g]
MA[h]	3	0.451 ± 0.011	0.531 ± 0.012	0.860 ± 0.008	0.887 ± 0.005	0.766 ± 0.062
CoMFA	4	0.490 ± 0.015	0.577 ± 0.017	0.843 ± 0.010	0.872 ± 0.007	0.967 ± 0.089
	5	0.525 ± 0.014	0.617 ± 0.017	0.831 ± 0.011	0.859 ± 0.007	1.125 ± 0.090
CoMSIA	3	0.541 ± 0.011	0.617 ± 0.013	0.788 ± 0.009	0.839 ± 0.006	0.690 ± 0.095
	4	0.567 ± 0.013	0.668 ± 0.015	0.779 ± 0.010	0.828 ± 0.007	0.935 ± 0.106
	5	0.552 ± 0.022	0.650 ± 0.026	0.806 ± 0.018	0.842 ± 0.012	1.120 ± 0.126
model 3[i]	1	0.362 ± 0.008	0.426 ± 0.009	0.895 ± 0.005	0.917 ± 0.003	0.589 ± 0.049
CoMFA	2	0.574 ± 0.009	0.675 ± 0.010	0.745 ± 0.006	0.814 ± 0.005	1.014 ± 0.058
	3	0.587 ± 0.013	0.691 ± 0.015	0.746 ± 0.011	0.810 ± 0.008	1.228 ± 0.088
CoMSIA	1	0.518 ± 0.009	0.609 ± 0.010	0.778 ± 0.006	0.841 ± 0.004	0.602 ± 0.057
	2	0.580 ± 0.013	0.682 ± 0.015	0.739 ± 0.010	0.809 ± 0.007	0.807 ± 0.061
	3	0.548 ± 0.015	0.645 ± 0.017	0.780 ± 0.011	0.834 ± 0.008	1.015 ± 0.110

[a] Values are presented as mean ± SD (standard deviation) of 20 independent scrambling tests. [b] Number of PLS components. [c] Predictivity at the critical threshold level of perturbation s; $s = 0.85$; maximum value of $Q_s^{*2} = s$. [d] $Q_0^{*2} = Q_s^{*2}/s$; adjusted Q_s^{*2}, corresponding to the value expected for an unperturbed, nonredundant model, i.e., "classical" q^2. [e] Standard error of prediction at the critical threshold level of perturbation s. [f] $SDEP_0^* = \{[(2 - s)(n - N - 1)(SDEP_s^*) - (1 - s)(n - 1)SD_y^2]/(n - N - 1)\}^{1/2}$; $n = 31$ (number of ligands); $SD_y = 1.1$ (response standard deviation); adjusted $SDEP_s^*$, corresponding to the value expected for an unperturbed, nonredundant model. [g] Sensitivity to perturbation at s. [h] *M*anual *A*lignment model. [i] Model based on the docking alignment at the CB1 comparative model 3 (see ref 48).

out (LHO) cross-validation. In particular, the LHO method has been reported to give a good estimate of model predictivity.[73,88] The LSO method resulted in slightly lower q^2 values than LOO (0.535−0.695 vs 0.662−0.736, respectively), whereas the LHO cross-validation gave the lowest q^2 values but these were still significant (0.455−0.555).

In addition, the progressive scrambling procedure was applied to the QSAR models. This novel validation technique was developed to address the overly optimistic cross-validation or response randomization results for redundant data sets.[52,53] In this approach, small random perturbations are introduced into a data set. This causes the nominal predictivity of unstable models to fall off rapidly, whereas robust models are relatively stable. Both MA and DA3 models were shown to be stable, and the adjusted statistical values Q_0^{*2} and $SDEP_0^*$ were comparable with the corresponding q^2 and S_{PRESS} of cross-validation (Table 3). The third characteristic statistic from progressive scrambling is the instantaneous slope of the predictivity with respect to the degree of perturbation ($dq^2/dr^2_{yy'}$). It depicts the model sensitivity to perturbation at a critical threshold level of perturbation (here 0.85).[53] This value is reported to be a reliable indicator of model complexity, and thus, it helps to avoid overfitting due to too many PLS components. Specifically, a number of PLS components yielding a $dq^2/dr^2_{yy'}$ slope near unity should be optimal.

In the MA CoMFA model, the S_{PRESS} value was at minimum either at three components (LHO) or at five components (LSO, LOO). The q^2 value was significant already at three components but, as is generally the case, it became even higher when more complexity was added to the model. How many components can be used without fitting only noise? Progressive scrambling results suggested that four components would be optimal as the slope was only 0.766 with three components. The fourth component could be added to explain the data better without leading to overfitting (slope = 0.967), whereas five components would have already led to a slightly overfit model (slope > 1.1) even though $SDEP_0^*$ was the lowest at this level of complexity. Also for MA CoMSIA model, the progressive scrambling results indicated that a four-component model would be most robust ($SDEP_0^*$ at minimum, slope = 0.935) even though S_{PRESS} was smallest at five components (LSO, LOO) or at only one component (LHO). At one component only, the slope was still insignificant, while at five components the slope exceeded 1.1, revealing the overfitting.

In the DA3 CoMFA model, the S_{PRESS} value was lowest with three components but the progressive scrambling data showed that it lead to severe overfitting (slope > 1.2) even though q^2 and Q_0^{*2} were still greater than in the two-component model. Thus, we chose to use two components in the final, nonvalidated model. In the case of the DA3 CoMSIA model, both cross-validation and progressive scrambling data suggested that two components were optimal. If more complexity was added, Q_0^{*2} declined and $SDEP_0^*$ started to increase. Our study confirms that both the LHO procedure and progressive scrambling are efficient validation methods when assessing the predictivity of a QSAR model. In addition, progressive scrambling effectively reveals overfitting and model instability due to redundancy (see Supporting Information, sections J and K for an example). The experimental vs predicted pEC_{50} values of the final, nonvalidated CoMFA and CoMSIA models are provided in Supporting Information (section L).

CoMFA and CoMSIA fields. See Supporting Information (section N) for the field contributions. The resulting CoMFA and CoMSIA fields for MA and DA3 final models are shown in Figure 4. Compounds **4** and **19** serve as templates in the QSAR contour plots. In the MA model, both CoMFA and CoMSIA electrostatic fields suggest that a negative charge near the **19** carbonyl group and either a positive charge or a decrease in the negative charge further in the headgroup region would be favorable for activity (Figure 4A,B). In the DA3 CoMFA model there are unfavorable regions for a negative charge (blue) surrounding the endocannabinoid headgroup and a region favoring a negative charge (red) in the end of the headgroup moiety (Figure 4G). When comparing the fields to the receptor structure, the red favorable region matches with the hydroxyl group of T3.37(201) and the blue areas are in the proximity of the aromatic residues W6.48(356), F5.43(279), and F3.36(200). Both CoMFA and CoMSIA detect a negative-charge favorable region above the aromatic A ring of the cannabinoids (Figure 4G,H). This is immediately above the positively charged NZ and CE atoms of lysine K3.28(192). There are additional negative-charge favorable CoMFA fields surrounding the tricyclic cannabinoid structure due to the phenolic hydroxyl and pyran oxygens. The hydroxyl group of S7.39(383), for example, matches one of these regions. Two CoMSIA fields disfavoring a negative charge are located under the C10a atom of **4** and in the middle of the space occupied by the alkyl side chains of the ligands. The latter region is surrounded by the π-electron clouds of F3.25(189) and F2.64(177). In the MA model, the electrostatic fields are concentrated on the endocannabinoid headgroup region, whereas in the DA3 model there is more variance around the classical cannabinoid structures. This is most

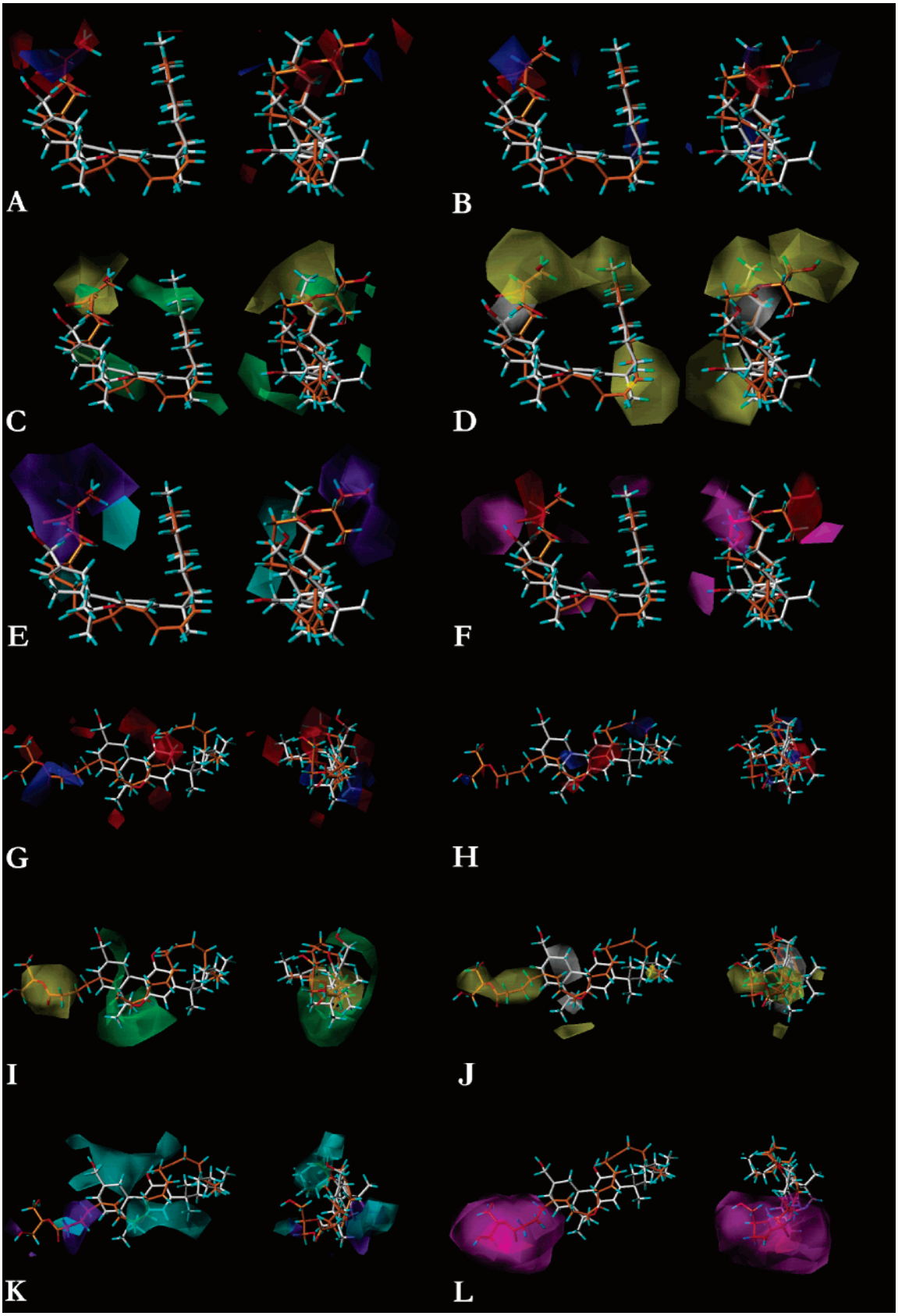

Figure 4. CoMFA and CoMSIA fields for the manual alignment model (A−F) and the docking alignment model at receptor model 3 (G−L). Molecules **19** (orange carbon atoms) and **4** (gray carbon atoms) serve as template structures. (A and G) CoMFA electrostatic fields: blue, negative-charge disfavored; red, negative-charge favored. (B and H) CoMSIA electrostatic fields: blue, negative-charge disfavored; red, negative-charge favored. (C and I) CoMFA steric fields: green, bulk favored; yellow, bulk disfavored. (D and J) CoMSIA hydrophobic fields: yellow, hydrophobic groups favored; white, hydrophobic groups disfavored. (E and K) CoMSIA hydrogen bond donor fields: cyan, donor favored; purple, donor disfavored; (F and L) CoMSIA acceptor fields: magenta, acceptor favored; red, acceptor disfavored.

likely due to the fuzzy alignment of the classical cannabinoid derivatives in the docking model.

For both alignment models, the steric CoMFA and CoMSIA fields are very similar and, therefore, only the CoMFA fields are shown in Figure 4C,I (see Supporting Information for the respective CoMSIA fields, section M). In the MA model, there are regions favoring steric bulk (green) near the two methyl groups of the DMH side chain as well as of the pyran ring. Steric bulk is favored also near the end of the alkyl side chain, emphasizing the optimal length of the side chain (5−7 carbons). CoMFA, but not CoMSIA, detects an additional sterically allowed region close to the phenolic hydroxyl group. Similarly, in the DA3 model, steric bulk is favored near the pyran methyl groups and, according to the CoMSIA fields, near the 1′,1′-dimethyl group as well. However, in both alignment models, steric bulk is disfavored in the middle of the endocannabinoid headgroup area. As already discussed above, the receptor subsite accommodating the endocannabinoid headgroup is fairly tight at that point, delineated by the aromatic residues. Naturally, as the potency of the endocannabinoid derivatives is in most cases lower than that of the classical cannabinoid derivatives, the area occupied by only the endocannabinoids will be penalized in the QSAR analyses. However, it is interesting that both the docking and manual alignments support the idea that the binding sites of the classical and endogenous cannabinoids overlap only partially. According to the present study, the difference in the binding sites could be due to a separate subsite reserved only for the endocannabinoid headgroup.

The CoMSIA hydrophobic fields in MA model (Figure 4D) show three large regions where the hydrophobic groups are favored (yellow): first, at the furthest end of the endocannabinoid headgroup, second, at the end of the alkyl side chain, and third, close to the 1′,1′-dimethyl group of the DMH side chain. These regions match well with the sterically favored areas of the steric CoMFA and CoMSIA contour plots. Hydrophobic groups are not favored (white) near the carbonyl oxygen of **19**, which is consistent with the negative-charge favorable region located in the same area. In the DA3 model, the whole endocannabinoid headgroup region is characterized by a narrow field favoring hydrophobicity (Figure 4J). As previously described, both hydrophobic and hydrophilic headgroups are allowed by the receptor. Delineating aromatic residues would, indeed, create such a microenvironment since they possess both hydrophobic and polar natures. Smaller regions in which the hydrophobic groups would increase activity are located near the pyran ring dimethyl and the 1′,1′,-dimethyl group of **4**. The two white regions describing where a hydrophobe would decrease activity are in the same points of the tricyclic system where an electrostatic charge would be beneficial for activity.

In the SYBYL implementation of CoMSIA, the donor fields describe where hydrogen bond acceptors should be located on the receptor, while the acceptor fields reveal where the corresponding H-bond donors should be on the receptor. According to the MA model, donor atoms are not favored (purple) in the end part of the endocannabinoid headgroup (Figure 4E), suggesting that there would be either a hydrophobic area or donating groups on the corresponding receptor site. The regions favoring a ligand donor atom (cyan) reveal the position for possible receptor acceptor atoms interacting with the phenolic hydroxyl and the NH of the amide bond in the most potent endocannabinoid derivatives such as **9**, **11**, **23**, and **25**. Acceptor fields of the MA model (Figure 4F) show that the carbonyl oxygen of most endocannabinoid derivatives and the C11 hydroxyl of **4** are located in a favorable position to interact with donating groups on the receptor. Experimental results from Khanolkar et al.[63] show that the carbonyl oxygen is important for the CB1 binding affinity of **17** and its analogues. They also suggest that the amide NH is involved in hydrogen bonding with the receptor. Acceptor-atom favoring fields (magenta) are displayed also near the phenolic hydroxyl (on the opposite side to the donor favoring field), in the end of the endocannabinoid headgroup and at the end of the alkyl side chain, suggesting a donor group on the complementary receptor site. Martin et al.[68] recently suggested that, at CB1, the phenolic oxygen of the THC derivatives would donate electrons rather than its hydrogen. An acceptor-atom disfavoring field (red) is positioned at the end part of the endocannabinoid headgroup region, agreeing well with the negative-charge unfavorable area of the electrostatic fields.

In the DA3 model, there are large continuous donor favoring areas around the classical cannabinoid tricyclic skeleton (Figure 4K). These areas correspond to the different hydroxyl groups of the ligands (phenolic hydroxyl, C1/C11 hydroxyl of **3** and **4**, SAH hydroxyl of **3**). At the receptor site there are the following possible acceptor groups in the very close proximity of the donor fields: hydroxyl of T3.33(197), backbone oxygen of L3.29(193), and hydroxyl of S7.39(383), of which actually only the serine S7.39 backbone oxygen forms a hydrogen bond with a docked ligand (**3**). One large region disfavoring donor groups is located in a relatively hydrophobic area at the beginning of the endocannabinoid acyl chain. There is a large acceptor favoring field covering the whole endocannabinoid headgroup area, and within that field there is a smaller unfavorable region accommodating carbonyl groups of some endocannabinoid derivatives (Figure 4L). At the receptor site, the former field embraces such H-bond donating residues as W5.43(279), W6.48(356), T3.37(201), and S5.48(284), while the latter field is located immediately in front of the NH of W6.48(356). On the whole, it seems that the hydrogen bond acceptor capacity would be important for the endocannabinoid headgroup area and the donor capacity for the classical cannabinoid derivatives.

Conclusions

In the present study, we examined the 3D-QSAR of a set of CB1 agonists representing both the endocannabinoid and classical cannabinoid structures. G-protein activation via CB1 served as the biological data. Both manual techniques and automated docking were used to build common alignments of the molecules. Maximal steric overlap and matching the aliphatic side chains of the molecules were emphasized when building the manual alignment, while we deliberately did not try to superimpose any polar pharmacophoric elements of the structurally different ligands. Docking alignments were created by docking the ligands at the seven different CB1 receptor conformers that we have reported previously. Random-group cross-validation and progressive scrambling were successfully used to validate the resulting QSAR models.

Our study demonstrates that despite their limitations and inaccuracy, comparative models can be useful for creating unbiased alignments for 3D-QSAR. Though there may be other ways to model the CB1 binding site, for example with regard to the conformation of the E2 loop, we were able to produce robust 3D-QSAR models that fitted the experimental data by using the docking alignment of the studied CB1 agonists at our receptor model. Interestingly, the docking alignment based on receptor model 3 led to a type of superimposition of the CB1 ligands similar to what we had chosen for the manual alignment.

In both alignments, the endocannabinoid headgroup occupies a region that excludes the classical cannabinoid derivatives. While it has been difficult to find a common pharmacophore model for the polar groups of endocannabinoids and classical cannabinoids, our results suggest that these types of ligands seem only to partially overlap in the receptor binding site. Furthermore, both manual and docking-based alignments gave statistically similar QSAR models, though the docking-based models were less complex than the manually aligned models (two vs four components). In the absence of experimental 3D structures for the ligand−receptor complexes, it is not possible to define which ligand conformations would be the bioactive ones. In both cases, however, an internally consistent alignment of the ligands is a likely reason for the statistically robust models. Creating docking alignments is usually more straightforward than aligning ligands manually. This is the case especially with flexible molecules and when a common pharmacophore between different compound classes is unclear. Also, adding new, even structurally different compounds to the QSAR model can be simpler by docking than by a manual procedure.

To the authors' knowledge, this is the first time that data on potency (pEC_{50}) from G-protein activation has been successfully used to create statistically valid CoMFA and CoMSIA models for the CB1 ligands. In addition, our results confirm that the leave-half-out cross-validation and progressive scrambling methods efficiently reveal statistically unstable models and that progressive scrambling is a valuable tool in determining the number of optimal components used in a QSAR model. Finally, the resulting CoMFA and CoMSIA models can be utilized in rational drug design both to explain and predict the activity of novel endocannabinoid or classical cannabinoid structures.

Experimental Section

Chemicals. See Table 1 for the structures of the numbered molecules. Compound **1**, Δ^8-tetrahydrocannabinol (Δ^8-THC, **2**), and cannabinol (CBN, **7**) were purchased from Sigma (St. Louis, MO). Compounds **3**, **4**, **8**, **23** (ACPA), and **25** (ACEA) and the CB1 selective antagonist AM251 were obtained from Tocris Cookson Ltd (Bristol, U.K.). Compounds **5** (O-581-1) and **6** (O-572) were kindly donated by Prof. B. R. Martin (University of North Carolina, NC). Compounds **9** [(*R*)-16,16-dimethyl-docosa-*cis*-5,8,11,14-tetraenoyl-1′-hydroxy-2′-propylamide] and **11** (16,16-dimethyl-docosa-*cis*-5,8,11,14-tetraenoylethanolamide) were provided by Herbert Seltzman (RTI International, Research Triangle Park, NC). Compounds **10** (7,10,13,16-docosatetraenoylethanolamide) and **17** were obtained from Deva Biotech (Hatboro, PA). Compounds **12** (arachidonoyl trifluoromethyl ketone, ATFMK) and **19** were purchased from Cayman Chemical (Ann Arbor, MI), and **13** (2,2-dimethylanandamide) was purchased from Matreya, Inc. (Pleasant Gap, PA). Preparation of **14**, **16**, **18**, **20**, **22**, **24**, **27**−**32** is described elsewhere.[46,47,89] The sources for **15** (HU-313, 2-isopropoxyethyl ether), **21** (HU-310, 2-*O*-arachidonoyl glyceryl ether, noladin ether), **26** (*R*-methanandamide), and SR141716A appear in Savinainen et al.[90]

[^{35}S]GTPγS Membrane Binding Studies. CB1 dependent G-protein activities of the molecules **1**−**32** were determined using rat cerebellar membrane [^{35}S]GTPγS binding assay.[90] These studies were conducted using four-week-old male Wistar rats. All animal experiments were approved by the local ethics committee. The animals lived in a 12 h light/12 h dark cycle (lights on at 07:00 h) with water and food available ad libitum. The rats were decapitated 8 h after lights on (15:00 h), whole brains were removed, dipped in isopentane on dry ice, and stored at −80 °C. Preparation of rat cerebellar membranes and [^{35}S]GTPγS binding incubations with PMSF-pretreatment (1 mM) were carried out as previously described.[90] Maximal agonist responses (E_{max}, %basal) and potencies (pEC_{50}) were determined from the dose−response curves. CB1 dependent activity was confirmed by antagonizing half-maximal agonist responses with CB1 selective antagonists AM251 or SR141716 (1 μM). Results are presented as mean ± SEM of at least three independent experiments performed in duplicate. Data analysis was calculated as nonlinear regressions by GraphPad Prism 3.0.

Computational Methods. Construction of molecular structures, conformational analyses, energy minimization, and visualization were carried out in Tripos force field[91] using the molecular modeling package SYBYL.[92] Ligand structures were optimized by the steepest descent, Powell, and BFGS[93−96] methods. The genetic algorithm based program GOLD[97] was used for ligand docking, and CScore[98] module of SYBYL was used for relaxing, scoring, and ranking the resulting docking conformations. CoMFA[19] and CoMSIA,[49−51] as implemented in SYBYL, were used for generating the 3D-QSAR models.

Manual Alignment of Ligands. Crystal structures of arachidonic acid[99] and Δ^9-tetrahydrocannabinolic acid b[100] were taken as primary templates to construct the representative molecular structures of endogenous and classical cannabinoid derivatives, respectively. First, a systematic search was performed on the dimethylheptyl (DMH) side chain of **4**, the potent cannabinoid derivate chosen as a template for the manual alignment of all ligands. From every conformational family, a conformer with the lowest energy was optimized and placed into a database. Second, **19** was taken as a template structure for all endocannabinoid analogues. Structural and computational studies show that there are four low-energy conformers commonly identified for arachidonic acid: an angle-iron/extended conformation,[101,102] a hairpin/U-shaped conformation,[99] a J-shaped conformation,[103] and a helical conformation.[104] These ideal conformations were applied on **19** as defined by Reggio and Traore[105] (see Supporting Information, section B), and thereafter, distance-constrained[106] MD simulations[107] were run in a vacuum to determine realistic conformations of the ideal starting structures. One low-energy structure of each conformational shape was optimized, keeping the same distance constraints as above, and recorded into a database. Third, these four different shaped conformations of **19** were compared one by one with every representative of the conformational families of **4**. Molecules were superimposed upon each other by fitting their aliphatic side chains, and the common volume of the molecule pair was calculated (see Supporting Information, section C for the maximal volume overlaps of **4** with each shape of **19**). Also **3**, a potent bicyclic (nonclassical) cannabinoid structure and two semirigid alkyl amides that have been reported to activate G-protein via CB1 receptor[107] (see Supporting Information, section D) were compared in a similar manner with the different shaped conformers of **19**. Conformers of **3** were generated in a systematic search performed on the SAH (southern aliphatic hydroxyl; C4 hydroxypropyl) and DMH chains, whereas CONFORT (as implemented in SYBYL) was used to generate different conformers for the alkyl amides.

After comparing the resulting common volumes and the goodness of matching the pharmacophoric features for the molecule pairs, the U-shaped conformation of **19** was chosen to be the template for all the endocannabinoid derivatives. The MULTIFIT procedure of SYBYL was used to optimize the alignment of the U-shaped **19** and the respective conformer of **4**. The fitted atom pairs from **4** and **19** were C6′−C20, C5′−C19, C4−C12, C5−C11, C8−C6, and C9−C5, respectively. Subsequently, the other endocannabinoid structures were built according to the U-shaped conformer of **19** and then superimposed on **4** using the FIT ATOMS procedure for the respective atom pairs (as defined above). If the number of carbons in the aliphatic side chain varied from that of **4**, more attention had to be paid when choosing the correct atom pairs from the chain. The classical/nonclassical cannabinoid derivatives were superimposed on the template according to their tricyclic/bicyclic skeleton, and their aliphatic side chain was modified to adopt the same conformation as the template. All the aligned molecule structures were optimized so that the total energy (in the applied force field) did not exceed the local minimum by more than 4−5 kcal/mol.

Docking Alignments. The CB1 receptor models 1−7 reported previously by us[48] were used for creating docking alignments of the CB1 ligands. In each case, all ligands (**1**−**32**) were automatically docked into a cavity ($r = 18$ Å) surrounding the side-chain nitrogen of lysine K3.28(192). The docking program was allowed to produce maximally 25 different conformations for each ligand. Thereafter, the docking conformations were relaxed in the binding cleft and ranked according to CScore consensus scoring value. The best-ranked conformers were chosen for the 3D-QSAR models. However, if an endocannabinoid derivative was oriented in a way opposite to most others, the next best-ranked conformer, having the polar headgroup in the same direction as the other endocannabinoid derivatives, was taken instead.

Atomic Point Charges. Ab initio[108,109] charges were calculated for representative molecules of classical and endogenous cannabinoid derivatives and compared with several semiempirical[110] and topological charges.[111] The semiempirical MNDO (ESP fit)[112,113] charges, being the most similar to the ab initio charges, were applied on the data set molecules in their alignment conformation.

CoMFA and CoMSIA. CoMFA and CoMSIA methods were used to generate 3D-QSAR models for the different ligand alignments. For CoMFA, both elecrostatic and steric interaction fields and, for CoMSIA, steric, electrostatic, hydrophobic, H-bond acceptor, and H-bond donor similarity indices were calculated using the SYBYL default settings (sp^3 carbon probe, charge +1.0, grid spacing 2.0 Å). Column filtering was set to 2.0 kcal/mol. Measured potencies (pEC_{50}) were used as dependent variables. The resulting PLS models were validated both by leave-one-out (LOO) and random-group cross-validation (2 groups, leave-half-out, LHO; 5 groups, leave-some-out, LSO). Both LHO and LSO cross-validation procedures were repeated 20 times, and average statistical values were calculated. Also, a recently reported progressive scrambling[52,53] method was applied to the models. Evaluation of r_{yy}^2 (correlation between the original and scrambled responses) was conducted at the critical threshold level of perturbation $s = 0.85$. According to the CoMSIA field contributions (Supporting Information, section N) and the statistical values of QSAR models having only a single field or a limited combination of them (data not shown), we chose to use all CoMSIA field types in our final models. The number of components used in the final, nonvalidated models was chosen according to the validation results: concerning the lowest S_{PRESS} (standard error of prediction) or $SDEP_0$* (corresponding value from progressive scrambling), highest q^2 or Q_0*^{2} (corresponding value from progressive scrambling), complexity of the CoMFA/CoMSIA contour maps, and sensitivity to perturbation in the scrambling test. The default contour levels (80% for favored feature and 20% for disfavored feature) were used when viewing the QSAR (stdev * coeff) fields.

Amino Acid Numbering. Ballesteros and Weinstein's amino acid numbering scheme[114] is used in the text to refer to CB1 residues. For instance, W6.48(356) denotes a tryptophan residue in the sixth TM helix at sequence number 356, located two residues before (.48) the most highly conserved residue (.50) of the TM domain.

Acknowledgment. This work was supported by ISB (The National Graduate School in Informational and Structural Biology) and National Technology Agency of Finland. CSC − Scientific Computing, Ltd., is gratefully acknowledged for computational resources. We are grateful to Prof. Billy R. Martin (University of North Carolina) for providing **5** and **6**. We also thank Dr. Robert D. Clark for helpful correspondence concerning the progressive scrambling results, and Toni Rönkkö (M.Sc.), Ms. Taija Saarinen, Mrs. Helly Rissanen, and Mrs. Minna Glad for their technical assistance.

Supporting Information Available: Detailed results for the CB1 mediated G-protein activation by CB1 agonists, ideal torsion angles for different conformers of arachidonic acid, maximal overlap volumes of **4** with four different conformers of **19**, figure on classical cannabinoids docked at model 3, statistics of all CoMFA and CoMSIA PLS analyses, experimental vs predicted pEC_{50} values of CoMFA and CoMSIA models, CoMFA and CoMSIA field contributions, coordinates of the receptor model 3, and both the manual and docking alignments of the CB1 agonists. This material is available free of charge via the Internet at http://pubs.acs.org.

References

(1) Mechoulam, R. The Pharmacohistory of *Cannabis sativa*. In *Cannabinoids as therapeutic agents*; Mechoulam, R., Ed.; CRC Press: Boca Raton, FL, 1986; pp 1−19.
(2) Gaoni, Y.; Mechoulam, R. Isolation, Structure, and Partial Synthesis of an Active Constituent of Hashish. *J. Am. Chem. Soc.* **1964**, *86*, 1646−1647.
(3) Razdan, R. K. Structure−activity relationships in cannabinoids. *Pharmacol. Rev.* **1986**, *38*, 75−149.
(4) Johnson, M. R.; Melvin, L. S. The discovery of nonclassical cannabinoid analgetics. In *Cannabinoids As Therapeutic Agents*; Mechoulam, R., Ed.; CRC Press Inc.: Boca Raton, FL, 1986; pp 121−145.
(5) Pacheco, M.; Childers, S. R.; Arnold, R.; Casiano, F.; Ward, S. J. Aminoalkylindoles: actions on specific G-protein-linked receptors. *J. Pharmacol. Exp. Ther.* **1991**, *257*, 170−183.
(6) Matsuda, L. A.; Lolait, S. J.; Brownstein, M. J.; Young, A. C.; Bonner, T. I. Structure of a cannabinoid receptor and functional expression of the cloned cDNA. *Nature* **1990**, *346*, 561−564.
(7) Munro, S.; Thomas, K. L.; Abu-Shaar, M. Molecular characterization of a peripheral receptor for cannabinoids. *Nature* **1993**, *365*, 61−65.
(8) Devane, W. A.; Hanus, L.; Breuer, A.; Pertwee, R. G.; Stevenson, L. A.; Griffin, G.; Gibson, D.; Mandelbaum, A.; Etinger, A.; Mechoulam, R. Isolation and structure of a brain constituent that binds to the cannabinoid receptor. *Science* **1992**, *258*, 1946−1949.
(9) Mechoulam, R.; Ben-Shabat, S.; Hanus, L.; Ligumsky, M.; Kaminski, N. E.; Schatz, A. R.; Gopher, A.; Almog, S.; Martin, B. R.; Compton, D. R.; Pertwee, R. G.; Griffin, G.; Bayewitch, M.; Barg, J.; Vogel, Z. Identification of an endogenous 2-monoglyceride, present in canine gut, that binds to cannabinoid receptors. *Biochem. Pharmacol.* **1995**, *50*, 83−90.
(10) Sugiura, T.; Kondo, S.; Sukagawa, A.; Nakane, S.; Shinoda, A.; Itoh, K.; Yamashita, A.; Waku, K. 2-Arachidonoylglycerol: a possible endogenous cannabinoid receptor ligand in brain. *Biochem. Biophys. Res. Commun.* **1995**, *215*, 89−97.
(11) Hanus, L.; Abu-Lafi, S.; Fride, E.; Breuer, A.; Vogel, Z.; Shalev, D. E.; Kustanovich, I.; Mechoulam, R. 2-Arachidonyl glyceryl ether, an endogenous agonist of the cannabinoid CB1 receptor. *Proc. Natl. Acad. Sci. U.S.A.* **2001**, *98*, 3662−3665.
(12) Huang, S. M.; Bisogno, T.; Trevisani, M.; Al-Hayani, A.; De Petrocellis, L.; Fezza, F.; Tognetto, M.; Petros, T. J.; Krey, J. F.; Chu, C. J.; Miller, J. D.; Davies, S. N.; Geppetti, P.; Walker, J. M.; Di Marzo, V. An endogenous capsaicin-like substance with high potency at recombinant and native vanilloid VR1 receptors. *Proc. Natl. Acad. Sci. U.S.A.* **2002**, *99*, 8400−8405.
(13) Porter, A. C.; Sauer, J. M.; Knierman, M. D.; Becker, G. W.; Berna, M. J.; Bao, J.; Nomikos, G. G.; Carter, P.; Bymaster, F. P.; Leese, A. B.; Felder, C. C. Characterization of a novel endocannabinoid, virodhamine, with antagonist activity at the CB1 receptor. *J. Pharmacol. Exp. Ther.* **2002**, *301*, 1020−1024.
(14) Cravatt, B. F.; Giang, D. K.; Mayfield, S. P.; Boger, D. L.; Lerner, R. A.; Gilula, N. B. Molecular characterization of an enzyme that degrades neuromodulatory fatty-acid amides. *Nature* **1996**, *384*, 83−87.
(15) Dinh, T. P.; Carpenter, D.; Leslie, F. M.; Freund, T. F.; Katona, I.; Sensi, S. L.; Kathuria, S.; Piomelli, D. Brain monoglyceride lipase participating in endocannabinoid inactivation. *Proc. Natl. Acad. Sci. U.S.A.* **2002**, *99*, 10819−10824.
(16) Di Marzo, V.; Bifulco, M.; De Petrocellis, L. The endocannabinoid system and its therapeutic exploitation. *Nat. Rev. Drug Discov.* **2004**, *3*, 771−784.
(17) Rinaldi-Carmona, M.; Barth, F.; Heaulme, M.; Shire, D.; Calandra, B.; Congy, C.; Martinez, S.; Maruani, J.; Neliat, G.; Caput, D.; Ferrara, P.; Soubrie, P.; Breliere, J.-C.; le Fur, G. SR141716A, a potent and selective antagonist of the brain cannabinoid receptor. *FEBS Lett.* **1994**, *350*, 240−244.
(18) Reggio, P. H. Pharmacophores for ligand recognition and activation/inactivation of the cannabinoid receptors. *Curr. Pharm. Des.* **2003**, *9*, 1607−1633.

(19) Cramer, R. D., III; Patterson, D. E.; Bunce, J. D. Comparative Molecular Field Analysis (CoMFA). 1. Effect of Shape on Binding of Steroids to Carrier Proteins. *J. Am. Chem. Soc.* **1988**, *110*, 5959−5967.

(20) Keimowitz, A. R.; Martin, B. R.; Razdan, R. K.; Crocker, P. J.; Mascarella, S. W.; Thomas, B. F. QSAR analysis of Delta(8)-THC analogues: relationship of side-chain conformation to cannabinoid receptor affinity and pharmacological potency. *J. Med. Chem.* **2000**, *43*, 59−70.

(21) Francisco, M. E.; Seltzman, H. H.; Gilliam, A. F.; Mitchell, R. A.; Rider, S. L.; Pertwee, R. G.; Stevenson, L. A.; Thomas, B. F. Synthesis and structure−activity relationships of amide and hydrazide analogues of the cannabinoid CB(1) receptor antagonist N-(piperidinyl)-5-(4-chlorophenyl)-1-(2,4-dichlorophenyl)-4-methyl-1H-pyrazole-3-carboxamide (SR141716). *J. Med. Chem.* **2002**, *45*, 2708−2719.

(22) Shim, J. Y.; Welsh, W. J.; Cartier, E.; Edwards, J. L.; Howlett, A. C. Molecular interaction of the antagonist N-(piperidin-1-yl)-5-(4-chlorophenyl)-1-(2,4-dichlorophenyl)-4-methyl-1H-pyrazole-3-carboxamide with the CB1 cannabinoid receptor. *J. Med. Chem.* **2002**, *45*, 1447−1459.

(23) Shim, J. Y.; Collantes, E. R.; Welsh, W. J.; Subramaniam, B.; Howlett, A. C.; Eissenstat, M. A.; Ward, S. J. Three-dimensional quantitative structure−activity relationship study of the cannabimimetic (aminoalkyl)indoles using comparative molecular field analysis. *J. Med. Chem.* **1998**, *41*, 4521−4532.

(24) Tetko, I. V.; Kovalishyn, V. V.; Livingstone, D. J. Volume learning algorithm artificial neural networks for 3D QSAR studies. *J. Med. Chem.* **2001**, *44*, 2411−2420.

(25) Howlett, A. C.; Mukhopadhyay, S.; Shim, J. Y.; Welsh, W. J. Signal transduction of eicosanoid CB1 receptor ligands. *Life Sci.* **1999**, *65*, 617−625.

(26) Huffman, J. W.; Miller, J. R.; Liddle, J.; Yu, S.; Thomas, B. F.; Wiley: J. L.; Martin, B. R. Structure−activity relationships for 1′,1′-dimethylalkyl-Delta(8)-tetrahydrocannabinols. *Bioorg. Med. Chem.* **2003**, *11*, 1397−1410.

(27) Thomas, B. F.; Compton, D. R.; Martin, B. R.; Semus, S. F. Modeling the cannabinoid receptor: a three-dimensional quantitative structure−activity analysis. *Mol. Pharmacol.* **1991**, *40*, 656−665.

(28) Thomas, B. F.; Adams, I. B.; Mascarella, S. W.; Martin, B. R.; Razdan, R. K. Structure−activity analysis of anandamide analogs: relationship to a cannabinoid pharmacophore. *J. Med. Chem.* **1996**, *39*, 471−479.

(29) Schmetzer, S.; Greenidge, P.; Kovar, K. A.; Schulze-Alexandru, M.; Folkers, G. Structure−activity relationships of cannabinoids: a joint CoMFA and pseudoreceptor modelling study. *J. Comput.-Aided Mol. Des.* **1997**, *11*, 278−292.

(30) Fichera, M.; Cruciani, G.; Bianchi, A.; Musumarra, G. A 3D-QSAR study on the structural requirements for binding to CB(1) and CB(2) cannabinoid receptors. *J. Med. Chem.* **2000**, *43*, 2300−2309.

(31) Huffman, J. W.; Dai, D.; Martin, B. R.; Compton, D. R. Design, synthesis and pharmacology of cannabimimetic indoles. *Bioorg. Med. Chem. Lett.* **1994**, *4*, 563−566.

(32) Dutta, A. K.; Ryan, W.; Thomas, B. F.; Singer, M.; Compton, D. R.; Martin, B. R.; Razdan, R. K. Synthesis, pharmacology, and molecular modeling of novel 4-alkyloxy indole derivatives related to cannabimimetic aminoalkyl indoles (AAIs). *Bioorg. Med. Chem.* **1997**, *5*, 1591−1600.

(33) Eissenstat, M. A.; Bell, M. R.; D'Ambra, T. E.; Alexander, E. J.; Daum, S. J.; Ackerman, J. H.; Gruett, M. D.; Kumar, V.; Estep, K. G.; Olefirowicz, E. M.; et al. Aminoalkylindoles: structure−activity relationships of novel cannabinoid mimetics. *J. Med. Chem.* **1995**, *38*, 3094−3105.

(34) Xie, X. Q.; Eissenstat, M.; Makriyannis, A. Common cannabimimetic pharmacophoric requirements between aminoalkyl indoles and classical cannabinoids. *Life Sci.* **1995**, *56*, 1963−1970.

(35) Tong, W.; Collantes, E. R.; Welsh, W. J.; Berglund, B. A.; Howlett, A. C. Derivation of a pharmacophore model for anandamide using constrained conformational searching and comparative molecular field analysis. *J. Med. Chem.* **1998**, *41*, 4207−4215.

(36) Thomas, B. F.; Gilliam, A. F.; Burch, D. F.; Roche, M. J.; Seltzman, H. H. Comparative receptor binding analyses of cannabinoid agonists and antagonists. *J. Pharmacol. Exp. Ther.* **1998**, *285*, 285−292.

(37) Ooms, F.; Wouters, J.; Oscari, O.; Happaerts, T.; Bouchard, G.; Carrupt, P. A.; Testa, B.; Lambert, D. M. Exploration of the pharmacophore of 3-alkyl-5-arylimidazolidinediones as new CB(1) cannabinoid receptor ligands and potential antagonists: synthesis, lipophilicity, affinity, and molecular modeling. *J. Med. Chem.* **2002**, *45*, 1748−1756.

(38) Compton, D. R.; Rice, K. C.; De Costa, B. R.; Razdan, R. K.; Melvin, L. S.; Johnson, M. R.; Martin, B. R. Cannabinoid structure−activity relationships: correlation of receptor binding and in vivo activities. *J. Pharmacol. Exp. Ther.* **1993**, *265*, 218−226.

(39) Griffin, G.; Williams, S.; Aung, M. M.; Razdan, R. K.; Martin, B. R.; Abood, M. E. Separation of cannabinoid receptor affinity and efficacy in delta-8-tetrahydrocannabinol side-chain analogues. *Br. J. Pharmacol.* **2001**, *132*, 525−535.

(40) Kenakin, T.; Onaran, O. The ligand paradox between affinity and efficacy: can you be there and not make a difference? *Trends Pharmacol. Sci.* **2002**, *23*, 275−280.

(41) Griffin, G.; Wray, E. J.; Martin, B. R.; Abood, M. E. Cannabinoid agonists and antagonists discriminated by receptor binding in rat cerebellum. *Br. J. Pharmacol.* **1999**, *128*, 684−688.

(42) Griffin, G.; Wray, E. J.; Rorrer, W. K.; Crocker, P. J.; Ryan, W. J.; Saha, B.; Razdan, R. K.; Martin, B. R.; Abood, M. E. An investigation into the structural determinants of cannabinoid receptor ligand efficacy. *Br. J. Pharmacol.* **1999**, *126*, 1575−1584.

(43) Rivara, S.; Mor, M.; Silva, C.; Zuliani, V.; Vacondio, F.; Spadoni, G.; Bedini, A.; Tarzia, G.; Lucini, V.; Pannacci, M.; Fraschini, F.; Plazzi, P. V. Three-dimensional quantitative structure−activity relationship studies on selected MT1 and MT2 melatonin receptor ligands: requirements for subtype selectivity and intrinsic activity modulation. *J. Med. Chem.* **2003**, *46*, 1429−1439.

(44) Song, Z. H.; Bonner, T. I. A lysine residue of the cannabinoid receptor is critical for receptor recognition by several agonists but not WIN55212-2. *Mol. Pharmacol.* **1996**, *49*, 891−896.

(45) McAllister, S. D.; Rizvi, G.; Anavi-Goffer, S.; Hurst, D. P.; Barnett-Norris, J.; Lynch, D. L.; Reggio, P. H.; Abood, M. E. An aromatic microdomain at the cannabinoid CB(1) receptor constitutes an agonist/inverse agonist binding region. *J. Med. Chem.* **2003**, *46*, 5139−5152.

(46) Parkkari, T.; Savinainen, J. R.; Mäkipaja, L.; Sirviö, T.; Saario, S. M.; Laitinen, J. T.; Nevalainen, T.; Niemi, R.; Järvinen, T. Synthesis, CB1 receptor activities and enzymatic stability of reversed amide derivatives of arachidonoyl ethanol amide. Submitted 2005.

(47) Parkkari, T.; Salo, O. M. H.; Huttunen, K.; Savinainen, J. R.; Laitinen, J. T.; Poso, A.; Nevalainen, T.; Järvinen, T. Synthesis and CB1 receptor activities of dimethylheptyl derivatives of 2-arachidonoyl glycerol (2-AG) and 2-arachidonyl glyceryl ether (2-AGE). *Biorg. Med. Chem.* In press.

(48) Salo, O. M.; Lahtela-Kakkonen, M.; Gynther, J.; Jarvinen, T.; Poso, A. Development of a 3D model for the human cannabinoid CB1 receptor. *J. Med. Chem.* **2004**, *47*, 3048−3057.

(49) Böhm, M.; Stürzebecher, J.; Klebe, G. Three-dimensional quantitative structure−activity relationship analyses using comparative molecular field analysis and comparative molecular similarity indices analysis to elucidate selectivity differences of inhibitors binding to trypsin, thrombin, and factor Xa. *J. Med. Chem.* **1999**, *42*, 458−477.

(50) Klebe, G.; Abraham, U. Comparative molecular similarity index analysis (CoMSIA) to study hydrogen-bonding properties and to score combinatorial libraries. *J. Comput.-Aided Mol. Des.* **1999**, *13*, 1−10.

(51) Klebe, G.; Abraham, U.; Mietzner, T. Molecular similarity indices in a comparative analysis (CoMSIA) of drug molecules to correlate and predict their biological activity. *J. Med. Chem.* **1994**, *37*, 4130−4146.

(52) Clark, R. D.; Sprous, D. G.; Leonard, J. M. *Validating models based on large data sets*; Prous Science: Barcelona, 2001; p 475−485.

(53) Clark, R. D.; Fox, P. C. Statistical variation in progressive scrambling. *J. Comput.-Aided Mol. Des.* **2004**, *17*, 1−14.

(54) Sugiura, T.; Kodaka, T.; Nakane, S.; Miyashita, T.; Kondo, S.; Suhara, Y.; Takayama, H.; Waku, K.; Seki, C.; Baba, N.; Ishima, Y. Evidence that the cannabinoid CB1 receptor is a 2-arachidonoylglycerol receptor. Structure−activity relationship of 2-arachidonoylglycerol, ether-linked analogues, and related compounds. *J. Biol. Chem.* **1999**, *274*, 2794−2801.

(55) Ryan, W. J.; Banner, W. K.; Wiley, J. L.; Martin, B. R.; Razdan, R. K. Potent anandamide analogs: the effect of changing the length and branching of the end pentyl chain. *J. Med. Chem.* **1997**, *40*, 3617−3625.

(56) Seltzman, H. H.; Fleming, D. N.; Thomas, B. F.; Gilliam, A. F.; McCallion, D. S.; Pertwee, R. G.; Compton, D. R.; Martin, B. R. Synthesis and pharmacological comparison of dimethylheptyl and pentyl analogs of anandamide. *J. Med. Chem.* **1997**, *40*, 3626−3634.

(57) Berglund, B. A.; Fleming, P. R.; Rice, K. C.; Shim, J. Y.; Welsh, W. J.; Howlett, A. C. Development of a novel class of monocyclic and bicyclic alkyl amides that exhibit CB1 and CB2 cannabinoid receptor affinity and receptor activation. *Drug Des. Discov.* **2000**, *16*, 281−294.

(58) Busch-Petersen, J.; Hill, W. A.; Fan, P.; Khanolkar, A.; Xie, X. Q.; Tius, M. A.; Makriyannis, A. Unsaturated side chain beta-11-hydroxyhexahydrocannabinol analogs. *J. Med. Chem.* **1996**, *39*, 3790−3796.

(59) Xie, X. Q.; Melvin, L. S.; Makriyannis, A. The conformational properties of the highly selective cannabinoid receptor ligand CP-55,940. *J. Biol. Chem.* **1996**, *271*, 10640−10647.

(60) Khanolkar, A. D.; Lu, D.; Fan, P.; Tian, X.; Makriyannis, A. Novel conformationally restricted tetracyclic analogs of delta8-tetrahydrocannabinol. *Bioorg. Med. Chem. Lett.* **1999**, *9*, 2119−2124.
(61) Barnett-Norris, J.; Guarnieri, F.; Hurst, D. P.; Reggio, P. H. Exploration of biologically relevant conformations of anandamide, 2-arachidonylglycerol, and their analogues using conformational memories. *J. Med. Chem.* **1998**, *41*, 4861−4872.
(62) Barnett-Norris, J.; Hurst, D. P.; Lynch, D. L.; Guarnieri, F.; Makriyannis, A.; Reggio, P. H. Conformational memories and the endocannabinoid binding site at the cannabinoid CB1 receptor. *J. Med. Chem.* **2002**, *45*, 3649−3659.
(63) Khanolkar, A. D.; Abadji, V.; Lin, S.; Hill, W. A.; Taha, G.; Abouzid, K.; Meng, Z.; Fan, P.; Makriyannis, A. Headgroup analogs of arachidonylethanolamide, the endogenous cannabinoid ligand. *J. Med. Chem.* **1996**, *39*, 4515−4519.
(64) Johnson, M. R.; Melvin, L. S.; Althuis, T. H.; Bindra, J. S.; Harbert, C. A.; Milne, G. M.; Weissman, A. Selective and potent analgetics derived from cannabinoids. *J. Clin. Pharmacol.* **1981**, *21*, 271S−282S.
(65) Huffman, J. W.; Yu, S.; Showalter, V.; Abood, M. E.; Wiley: J. L.; Compton, D. R.; Martin, B. R.; Bramblett, R. D.; Reggio, P. H. Synthesis and pharmacology of a very potent cannabinoid lacking a phenolic hydroxyl with high affinity for the CB2 receptor. *J. Med. Chem.* **1996**, *39*, 3875−3877.
(66) Pinto, J. C.; Potie, F.; Rice, K. C.; Boring, D.; Johnson, M. R.; Evans, D. M.; Wilken, G. H.; Cantrell, C. H.; Howlett, A. C. Cannabinoid receptor binding and agonist activity of amides and esters of arachidonic acid. *Mol. Pharmacol.* **1994**, *46*, 516−522.
(67) Sheskin, T.; Hanus, L.; Slager, J.; Vogel, Z.; Mechoulam, R. Structural requirements for binding of anandamide-type compounds to the brain cannabinoid receptor. *J. Med. Chem.* **1997**, *40*, 659−667.
(68) Martin, B. R.; Jefferson, R. G.; Winckler, R.; Wiley, J. L.; Thomas, B. F.; Crocker, P. J.; Williams, W.; Razdan, R. K. Assessment of structural commonality between tetrahydrocannabinol and anandamide. *Eur. J. Pharmacol.* **2002**, *435*, 35−42.
(69) Huffman, J. W.; Lu, J.; Hynd, G.; Wiley, J. L.; Martin, B. R. A pyridone analogue of traditional cannabinoids. A new class of selective ligands for the CB(2) receptor. *Bioorg. Med. Chem.* **2001**, *9*, 2863−2870.
(70) Reggio, P. H.; Panu, A. M.; Miles, S. Characterization of a region of steric interference at the cannabinoid receptor using the active analog approach. *J. Med. Chem.* **1993**, *36*, 1761−1771.
(71) Reggio, P. H.; Greer, K. V.; Cox, S. M. The importance of the orientation of the C9 substituent to cannabinoid activity. *J. Med. Chem.* **1989**, *32*, 1630−1635.
(72) Sippl, W. Receptor-based 3D QSAR analysis of estrogen receptor ligands− merging the accuracy of receptor-based alignments with the computational efficiency of ligand-based methods. *J. Comput.-Aided. Mol. Des.* **2000**, *14*, 559−572.
(73) Tervo, A. J.; Nyronen, T. H.; Ronkko, T.; Poso, A. A structure−activity relationship study of catechol-O-methyltransferase inhibitors combining molecular docking and 3D QSAR methods. *J. Comput.-Aided Mol. Des.* **2003**, *17*, 797−810.
(74) Tervo, A. J.; Nyronen, T. H.; Ronkko, T.; Poso, A. Comparing the quality and predictiveness between 3D QSAR models obtained from manual and automated alignment. *J. Chem. Inf. Comput. Sci.* **2004**, *44*, 807−816.
(75) Soderholm, A. A.; Lehtovuori, P. T.; Nyronen, T. H. Three-dimensional structure−activity relationships of nonsteroidal ligands in complex with androgen receptor ligand-binding domain. *J. Med. Chem.* **2005**, *48*, 917−925.
(76) Xu, Y.; Liu, H.; Niu, C.; Luo, C.; Luo, X.; Shen, J.; Chen, K.; Jiang, H. Molecular docking and 3D QSAR studies on 1-amino-2-phenyl-4-(piperidin-1-yl)-butanes based on the structural modeling of human CCR5 receptor. *Bioorg. Med. Chem.* **2004**, *12*, 6193−6208.
(77) Kunick, C.; Lauenroth, K.; Wieking, K.; Xie, X.; Schultz, C.; Gussio, R.; Zaharevitz, D.; Leost, M.; Meijer, L.; Weber, A.; Jorgensen, F. S.; Lemcke, T. Evaluation and comparison of 3D-QSAR CoMSIA models for CDK1, CDK5, and GSK-3 inhibition by paullones. *J. Med. Chem.* **2004**, *47*, 22−36.
(78) Tikhonova, I. G.; Baskin, II.; Palyulin, V. A.; Zefirov, N. S. CoMFA and homology-based models of the glycine binding site of N-methyl-d-aspartate receptor. *J. Med. Chem.* **2003**, *46*, 1609−1616.
(79) Palczewski, K.; Kumasaka, T.; Hori, T.; Behnke, C. A.; Motoshima, H.; Fox, B. A.; Le Trong, I.; Teller, D. C.; Okada, T.; Stenkamp, R. E.; Yamamoto, M.; Miyano, M. Crystal structure of rhodopsin: A G protein-coupled receptor. *Science* **2000**, *289*, 739−745.
(80) McAllister, S. D.; Hurst, D. P.; Barnett-Norris, J.; Lynch, D.; Reggio, P. H.; Abood, M. E. Structural mimicry in class A G protein-coupled receptor rotamer toggle switches: the importance of the F3.36(201)/W6.48(357) interaction in cannabinoid CB1 receptor activation. *J. Biol. Chem.* **2004**, *279*, 48024−48037.
(81) Bissantz, C. Conformational changes of G protein-coupled receptors during their activation by agonist binding. *J. Recept. Signal Transduct. Res.* **2003**, *23*, 123−153.
(82) Lin, S.; Khanolkar, A. D.; Fan, P.; Goutopoulos, A.; Qin, C.; Papahadjis, D.; Makriyannis, A. Novel analogues of arachidonylethanolamide (anandamide): affinities for the CB1 and CB2 cannabinoid receptors and metabolic stability. *J. Med. Chem.* **1998**, *41*, 5353−5361.
(83) Jarrahian, A.; Manna, S.; Edgemond, W. S.; Campbell, W. B.; Hillard, C. J. Structure−activity relationships among N-arachidonylethanolamine (Anandamide) head group analogues for the anandamide transporter. *J. Neurochem.* **2000**, *74*, 2597−2606.
(84) Seltzman, H. H. Structure and receptor activity for classical cannabinoids. *Curr. Med. Chem.* **1999**, *6*, 685−704.
(85) Gallivan, J. P.; Dougherty, D. A. Cation-pi interactions in structural biology. *Proc. Natl. Acad. Sci. U.S.A.* **1999**, *96*, 9459−9464.
(86) Golbraikh, A.; Tropsha, A. Beware of q2! *J. Mol. Graph. Model.* **2002**, *20*, 269−276.
(87) Hawkins, D. M.; Basak, S. C.; Mills, D. Assessing model fit by cross-validation. *J. Chem. Inf. Comput. Sci.* **2003**, *43*, 579−586.
(88) Oprea, T. I.; Garcia, A. E. Three-dimensional quantitative structure−activity relationships of steroid aromatase inhibitors. *J. Comput.-Aided Mol. Des.* **1996**, *10*, 186−200.
(89) Parkkari, T.; Savinainen, J. R.; Rauhala, A. L.; Tolonen, T. L.; Nevalainen, T.; Laitinen, J. T.; Gynther, J.; Jarvinen, T. Synthesis and CB1 receptor activities of novel arachidonyl alcohol derivatives. *Bioorg. Med.* Chem. Lett. **2004**, *14*, 3231−3234.
(90) Savinainen, J. R.; Jarvinen, T.; Laine, K.; Laitinen, J. T. Despite substantial degradation, 2-arachidonoylglycerol is a potent full efficacy agonist mediating CB(1) receptor-dependent G-protein activation in rat cerebellar membranes. *Br. J. Pharmacol.* **2001**, *134*, 664−672.
(91) Clark, M.; Cramer, R. D., III; Van Opdenbosch, N. Validation of the General Purpose Tripos 5.2 Force Field. *J. Comput. Chem.* **1989**, *10*, 982−1012.
(92) *SYBYL v. 6.7, 6.9.2 and 7.0*, Tripos Associates, Inc.: St. Louis, MO. http://www.tripos.com/.
(93) Broyden, C. The Convergence of a Class of Double-Rank Minimization Algorithms. *J. Inst. Math. Appl.* **1970**, *6*, 76−90, 222−231.
(94) Flethcer, R. A New Approach to Variable Metric Algorithms. *Comput. J.* **1970**, *13*, 317−322.
(95) Goldfarb, D. A Family of Variable-Metric Methods Derived by Variational Means. *Math. Comput.* **1970**, *24*, 23−26.
(96) Shanno, D. Conditioning of Quasi-Newton Methods for Function Minimization. *Math. Comput.* **1970**, *24*, 647−656.
(97) *GOLD v. 2.0*, Cambridge Crystallographic Data Centre: Cambridge, U.K. http://www.ccdc.cam.ac.uk/products/life_sciences/gold/.
(98) *CScore*, Tripos Associates, Inc.: St. Louis, MO. http://www.tripos.com/sciTech/inSilicoDisc/virtualScreening/cscore.html#references.
(99) LaLonde, J. M.; Levenson, M. A.; Roe, J. J.; Bernlohr, D. A.; Banaszak, L. J. Adipocyte lipid-binding protein complexed with arachidonic acid. Titration calorimetry and X-ray crystallographic studies. *J. Biol. Chem.* **1994**, *269*, 25339−25347.
(100) Rosenqvist, E.; Ottersen, T. The crystal and molecular structure of delta-9-tetrahydrocannabinolic acid b. *Acta Chem. Scand. B* **1975**, *29*, 379−384.
(101) Ernst, J.; Sheldrick, W. S.; Fuhrhop, J.-H. The structures of the essential unsaturated fatty acids. Crystal structure of linoleic acid and evidence for the crystal structures of alpha-linolenic and arachidonic acid. *Z. Naturforsch.* **1979**, *34b*, 706−711.
(102) Rich, M. R. Conformational analysis of arachidonic and related fatty acids using molecular dynamics simulations. *Biochim. Biophys. Acta* **1993**, *1178*, 87−96.
(103) Corey, E. J.; Iguchi, S.; Albright, J.; De, B. Studies on the conformational mobility of arachidonic acid. Facile macrolactonization of 20-hydroxyarachidonic acid. *Tetrahedron Lett.* **1983**, *24*, 37−40.
(104) Leach, A. R.; Prout, K. Automated conformational analysis: directed conformational search using the A* algorithm. *J. Comput. Chem.* **1990**, *11*, 1193−1205.
(105) Reggio, P. H.; Traore, H. Conformational requirements for endocannabinoid interaction with the cannabinoid receptors, the anandamide transporter and fatty acid amidohydrolase. *Chem. Phys. Lipids* **2000**, *108*, 15−35.
(106) Atom pairs for distance constraints: U-shaped = 1−19, 3−17, 4−9, 12−14; J-shaped = 2−8, 3−11, 9−15, 7−20; extended = 2−19, 4−11; helical = 1−8, 7−13, 9−20. See Table 1 (molecule **19**) for atom numbering. Constrain constant = 100.00 for all shapes except for extended = 200.00.
(107) MD parameters: Tripos force field, charges = none, length = 100 ps, temperature = 500 K, step size = 2 fs, Bonds to SHAKE applied on hydrogen atoms, snapshot every 1 ps.

(108) *Gaussian 98*, Gaussian, Inc.: Wallingford, CT, 1998.
(109) Gaussian parameters: multiplicity = singlet; charges = Merz−Kollman; theory = Hartree−Fock; basis set = 3-21G*, geometry optimization = FULL; constrain charges to match dipole = YES.
(110) PM3, AM1, MNDO (ESP fit); computed via MOPAC v. 6.0 (QCPE No. 455) interface in SYBYL.
(111) Gasteiger, Gasteiger−Hückel, Pullman, Del-Re; computed as implemented in SYBYL.
(112) Dewar, M. J. S.; Thiel, W. Ground States of Molecules, 38. The MNDO Method. Approximations and Parameters. *J. Am. Chem. Soc.* **1977**, *99*, 4899−4907.
(113) Besler, B. H.; Merz, K. M.; Kollman, P. A. Atomic charges derived from semiempirical methods. *J. Comput. Chem.* **1990**, *11*, 431−439.
(114) Ballesteros, J. A.; Weinstein, H. W. Integrated methods for the construction of three-dimensional models and computational probing of structure−function relations in G-protein coupled receptors. In *Methods in Neuroscience*; Conn, P. M., Sealfon, S. C., Eds.; Academic Press: San Diego, 1995; Vol. 25, pp 366−428.
(115) Hurst, D. P.; Lynch, D. L.; Barnett-Norris, J.; Hyatt, S. M.; Seltzman, H. H.; Zhong, M.; Song, Z. H.; Nie, J.; Lewis, D.; Reggio, P. H. N-(piperidin-1-yl)-5-(4-chlorophenyl)-1-(2,4-dichlorophenyl)-4-methyl-1H-pyrazole-3-carboxamide (SR141716A) interaction with LYS 3.28(192) is crucial for its inverse agonism at the cannabinoid CB1 receptor. *Mol. Pharmacol.* **2002**, *62*, 1274−1287.

JM0505157